

NRC Publications Archive **Archives des publications du CNRC**

Characterizing Human Shape Variation Using 3-D Anthropometric Data

Ben Azouz, Zouhour; Rioux, Marc; Shu, Chang; Lepage, R.

This publication could be one of several versions: author's original, accepted manuscript or the publisher's version. / La version de cette publication peut être l'une des suivantes : la version prépublication de l'auteur, la version acceptée du manuscrit ou la version de l'éditeur.

Publisher's version / Version de l'éditeur:

The Visual Computer International Journal of Computer Graphics, 22, 5, 2005

NRC Publications Archive Record / Notice des Archives des publications du CNRC :

<https://nrc-publications.canada.ca/eng/view/object/?id=7693f8c4-8c82-48ee-908c-11ece7c0cd3c>
<https://publications-cnrc.canada.ca/fra/voir/objet/?id=7693f8c4-8c82-48ee-908c-11ece7c0cd3c>

Access and use of this website and the material on it are subject to the Terms and Conditions set forth at

<https://nrc-publications.canada.ca/eng/copyright>

READ THESE TERMS AND CONDITIONS CAREFULLY BEFORE USING THIS WEBSITE.

L'accès à ce site Web et l'utilisation de son contenu sont assujettis aux conditions présentées dans le site

<https://publications-cnrc.canada.ca/fra/droits>

LISEZ CES CONDITIONS ATTENTIVEMENT AVANT D'UTILISER CE SITE WEB.

Questions? Contact the NRC Publications Archive team at

PublicationsArchive-ArchivesPublications@nrc-cnrc.gc.ca. If you wish to email the authors directly, please see the first page of the publication for their contact information.

Vous avez des questions? Nous pouvons vous aider. Pour communiquer directement avec un auteur, consultez la première page de la revue dans laquelle son article a été publié afin de trouver ses coordonnées. Si vous n'arrivez pas à les repérer, communiquez avec nous à PublicationsArchive-ArchivesPublications@nrc-cnrc.gc.ca.





National Research
Council Canada

Institute for
Information Technology

Conseil national
de recherches Canada

Institut de technologie
de l'information

NRC-CNR

*Characterizing Human Shape Variation Using 3-D Anthropometric Data **

Ben Azouz, Z., Rioux, M., Shu, C., and Lepage, R.
September 2005

* published in The Visual Computer International Journal of Computer Graphics, volume 22, number 5, pp. 302-314. 2005. NRC 48265.

Copyright 2005 by
National Research Council of Canada

Permission is granted to quote short excerpts and to reproduce figures and tables from this report, provided that the source of such material is fully acknowledged.

Zouhour Ben Azouz
Marc Rioux
Chang Shu
Richard Lepage

Characterizing human shape variation using 3D anthropometric data

Published online: 21 April 2006
© Springer-Verlag 2006

Z. Ben Azouz (✉) · M. Rioux · C. Shu
National Research Council of Canada,
Institute of Information Technology, 1200
Montreal Road, Building M-50, Ottawa,
ON, Canada K1A 0R6
{Zouhour.benazouz; Marc.Rioux;
Chang.Shu}@nrc-cnrc.gc.ca

R. Lepage
École de Technologie Supérieure de
Montréal, 110 Rue Notre dame ouest,
Montréal, Québec, Canada H3C 1K3
Richard.Lepage@etsmtl.ca

Abstract Characterizing the variations of the human body shape is fundamentally important in many applications ranging from animation to product design. 3D scanning technology makes it possible to digitize the complete surfaces of a large number of human bodies, providing much richer information about the body shape than traditional anthropometric measurements. This technology opens up opportunities to extract new measurements for quantifying the body shape. In this paper, we present a new method for extracting the main modes of variations of the human shape from a 3D anthropometric database. Previous approaches rely on anatomical landmarks. Using a volumetric representation, we

show that human shape analysis can be performed despite the lack of such information. We first introduce a technique for repairing the 3D models from the original scans. Principal components analysis is then applied to the volumetric description of a set of human models to extract dominant components of shape variability for a target population. We demonstrate a good reconstruction of the original models from a reduced number of components. Finally, we provide tools for visualizing the main modes of human shape variation.

Keywords 3D anthropometry · Volumetric description · Human body modeling

1 Introduction

Characterizing and understanding human shape variation is traditionally the subject of anthropometry—the study of human body measurement. It is essential for better ergonomic design of any product with which people interact, such as clothing, automobiles, and workstations. Recently, researchers in the computer animation community have increasingly realized the importance of generating realistic virtual actors by capturing real human shapes [15].

The traditional anthropometry is based on a set of measurements corresponding to linear distances between anatomical landmarks and circumference values at predefined locations. These measurements provide limited in-

formation about the human body shape [19]. Furthermore, the traditional measurement, performed by hand, is a long and tedious process, requiring about 30 minutes for each subject. This presents a severe limitation for surveying a large number of subjects. Advances in surface digitization technology have led to the appearance of 3D surface anthropometry where whole body scanners are used to generate detailed human models in a few seconds.

Whole body scanners generate verbose data that cannot be used directly for shape analysis. Therefore, it is necessary to convert 3D scans to a compact representation that retains information about the body shape. Principal components analysis (PCA) is a potential answer to this need. The central issue in applying PCA to 3D anthropometric data is to bring all the models in correspondence to each other. This means that all models under consider-

ation have to be sampled with an equal number of points and every point in one model has a unique matching point in every other model.

In this paper, we propose to bring human models into correspondence with each other by converting their polygonal mesh descriptions to a volumetric representation. We align 3D scans inside a volume of fixed dimensions, which is sampled to a set of voxels. A human model is then characterized by an array of signed distances between the voxels and their nearest point on the body surface. Correspondence is achieved by comparing for each voxel the signed distances attributed to different models. Surfaces are reconstructed from the volumetric description using the marching cubes algorithm [14]. The main advantage of the volumetric representation is that correspondence between different models is achieved without using anatomical landmarks, thus avoiding a time-consuming process, since it requires placing markers at the landmark locations before scanning.

Principal components analysis is applied to the volumetric representation to extract a reduced number of components representing the main modes of variation of the human body. These components represent an orthogonal basis of the shape space and thus human models can be characterized compactly by their projections onto this basis. We show that some of these components correspond to commonly used body measurements, like height and weight, and that others indicate new ways of characterizing the body shape. We demonstrate that the intuitive meanings of these components are easily realized through visualizing the changes of the body shape along each main component. By interpreting the components, we provide insight into these new quantities, which may lead to more effective use of the shape variations in applications that need to compare, synthesize, recognize, and monitor human bodies.

The remainder of this paper is organized as follows. In the next section, we present a brief description of the CAESAR database, the surface anthropometric data used in this paper. Then, we review related work in human shape analysis, model repairing and voxelization. Next, we describe an algorithm for filling the holes in the models. This algorithm includes the voxelization of the human models. Then, we present the extraction of the main modes of variation in the human shape space using PCA. Finally, we discuss the results of our approach.

2 CAESAR database

CAESAR (Civilian American and European Surface Anthropometry Resource) was the first 3D surface anthropometry survey performed in the USA and Europe [18]. During this project, body measurements were taken from about 6000 civilians between the ages of 18 and 65 in the

USA, the Netherlands and Italy. Subjects were scanned in three postures wearing tight clothes and hair coverings. The Cyberware WB4 [7] and Vitronic [9] full-body scanners were used. Each generated 3D model contains around 300 000 triangles. A set of 74 white markers were placed at anatomical landmarks prior to scanning. The 3D locations of these landmarks were extracted from the range data using a semi-automatic approach [3].

Our experiments are based on a set of 3D human models in a standing posture from the CAESAR database.

3 Related work

In this section, we review related work in the areas of analyzing shape variability from 3D human scans, converting surfaces to volumetric representations (voxelization), and model repairing techniques.

The main problem in using 3D human scans for shape analysis is the large number of measured points and the lack of consistent representations between different models. A compact representation of human models can be found in [17] for applications related to the navigation and the visualization of 3D anthropometric databases. The proposed description is compact but does not allow the reconstruction of the original shape. Extended hyperquadrics are used in [2] to model human scans. Fitting extended hyperquadrics to 3D objects is time-consuming and a large number of coefficients are required to reconstruct detailed surfaces. Principal components analysis (PCA) has been widely used for shape analysis. For instance, in face recognition, PCA is used to extract a reduced number of components known as *eigenfaces* to represent the space of faces [13]. Applying the PCA to 3D anthropometric data requires bringing all the models in correspondence to each other. The most popular approach to establish this correspondence is based on fitting template models to measured scans such as in [20] and [1]. Anatomical landmarks are used for guiding the deformation of template surfaces to fit the scanned data. Most of the landmarks are difficult to detect without palpating the body and placing markers on the subjects prior to scanning. Unfortunately, this operation is time-consuming and thus will not be done in future anthropometric surveys. In this paper, we focus on human shape analysis without relying on anatomical landmarks. We propose to establish a correspondence between different models by converting their surfaces to a volumetric representation and analyze how the same volume is occupied by different models.

Voxelization is concerned with converting geometric objects from their continuous representations to a set of voxels. Early voxelization algorithms were binary, assigning 1 to the occupied voxels and 0 to the unoccupied ones [11, 12]. Rendered images using binary voxelization suffer from aliasing. Recently, alias-free voxelization

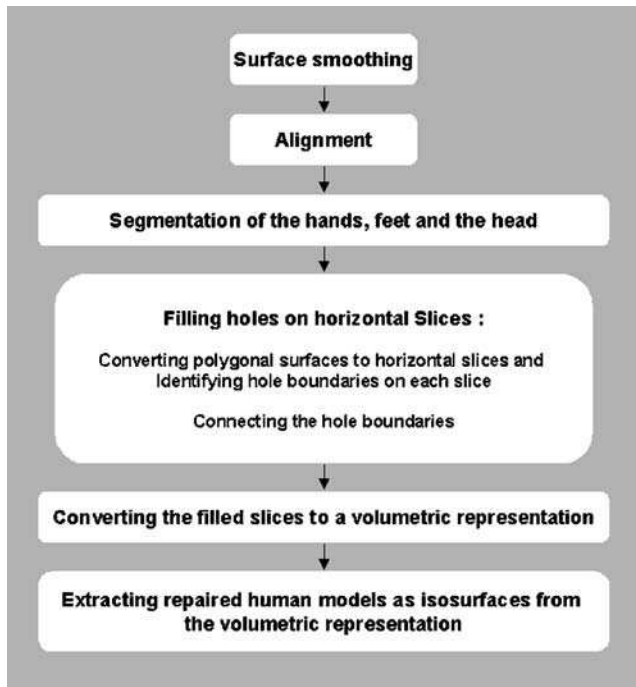


Fig. 1. Main steps of the hole-filling algorithm

techniques were proposed. They can be classified into two categories. The first one concerns filtering techniques where the problem of aliasing is solved by low-pass filtering [12, 24]. The second category concerns distance field techniques that assign to each voxel the distance to its nearest surface point [10]. This category is adequate for our application since it allows a description of the volume with a continuous function that can be used for a principal component analysis. Here, the cost of computing the signed-distance is a major concern.

Models from the CAESAR database are characterized by incomplete meshes due to occlusions and low grazing angles, as shown in Fig. 6. In order to compute an accurate distance field, it is necessary to repair these models. Several studies treated the problem of hole-filling in 3D models [4, 6]. These methods provide smooth hole filling, which is not adequate for the sole of the feet where bulbous shapes can be generated. Moreover, these techniques can produce bridges between the two legs and in the areas under the arms.

Since general hole-filling techniques cannot deal with the geometry of the human body, specific model repairing techniques have been developed. In [22], a toolbox for identifying holes in 3D human body scans is proposed. The basic idea is to detect and classify holes according to body segments. A potential use of the classification is to fit templates of body parts to missing areas. A library of body parts is then required. Moreover, fitting these parts to missing data is not straightforward. In the same spirit, the approach proposed in [1] efficiently solves the prob-

lem of hole filling by fitting a complete template surface to the CAESAR data. This technique is, however, based on anatomical landmarks.

We propose to repair the CAESAR models by estimating missing data from measured information using a slice-based method. The human models are sliced horizontally and hole-filling is performed by transforming each slice to a set of closed curves. This step is followed by generating a volumetric representation. The complete surface of a human body is extracted as an isosurface from the volumetric representation.

4 Hole-filling

To fill holes in a 3D model, we first intersect it with a set of horizontal planes. A watertight model should give closed curves in each slice. Otherwise, open curves indicate holes in the 3D model, and hole-filling is to close the curves, as shown in Fig. 5. The main steps of our hole-filling algorithm are summarized in the diagram of Fig. 1.

4.1 Surface smoothing

During hole-filling, the normal to the surface at each vertex around boundaries of the holes is used. Since the surface is particularly noisy in these areas, the models are smoothed using the Taubin filter [23] before hole-filling. This filter eliminates the noise while minimizing distortion of the original geometry. Surface smoothing of a 3D human model using the Taubin filter is illustrated in Fig. 2. The distribution of the distance between the original and the filtered models, computed using the PolyWorks [8] software, is characterized by a mean value of 0.4 mm and

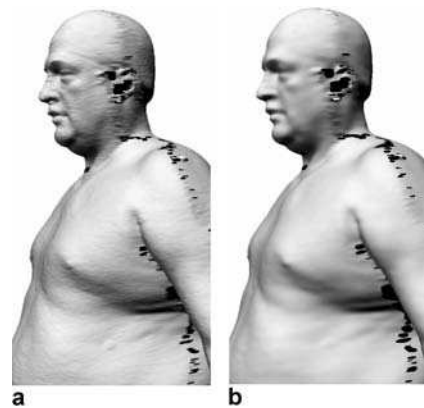


Fig. 2a,b. Surface smoothing of a 3D human scan using Taubin filter. **a** Original model. **b** Filtered model: the distribution of the displacement between the original and the filtered model is characterized by a mean value of 0.4 mm and a standard deviation of 0.52 mm

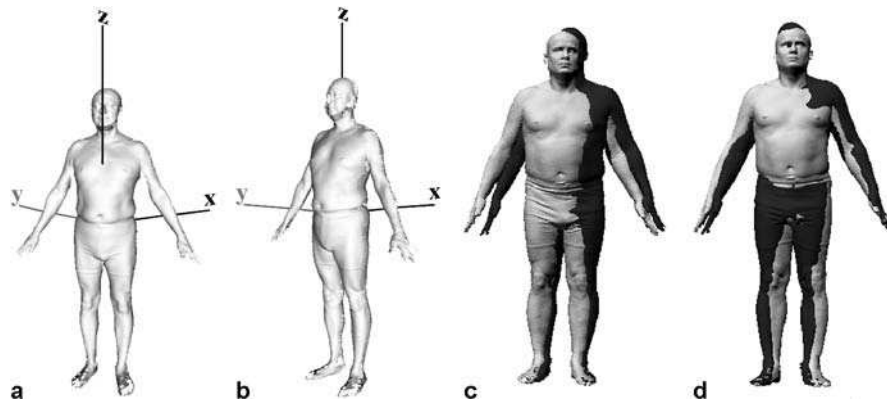


Fig. 3a-d. Reorientation of the 3D human models. **a** Original coordinate system. **b** Reoriented coordinate system. **c** Superposition of two original models. **d** Superposition of two aligned models

a standard deviation of 0.52 mm. This proves that there is no significant distortion after surface smoothing.

4.2 3D scans alignment

During the scanning process, subjects are asked to keep the same posture. Moreover, the platform of the used body scanners has marks where subjects should stand. Despite these precautions, 3D scans are not sufficiently aligned. This represents a source of noise that affects the shape analysis.

We minimize the misalignment by translating the human models so that their centres of gravity are vertically aligned. The 3D scans are then re-oriented so that the coordinate system corresponds to the principal axes of their tensor of inertia. We define X , Y , and Z axes as the direction of the thickness, width and height of the human body, respectively (Fig. 3(b)). The alignment of two human models is shown in Fig. 3(d).

4.3 Segmentation

A segmentation of the feet, hands and head is applied to the human models. This operation is useful for two reasons. First, the CAESAR models present a severe lack of data for the hands and hence, are not sufficient for the analysis of the hand shape. Thus, for our experiments we eliminate data corresponding to hands. Second, during the process of generating closed curves, slices are processed differently according to the body segment they belong to. Different criteria are used in order to avoid bridging between body segments beyond branching points, such as under the arms and between the legs. These criteria can be applied to most body parts. However, they complicate the hole-filling of the feet and the head. These segments are composed of scattered fragments of the true surface and are better repaired if they are considered simply as cylindrical objects without branching points.

After the alignment of the human models, it is simple to automatically delimit the hands and the feet with a set

of boxes. The feet are located from one side and the other in the X - Z plane (Fig. 4). For instance, the box delimiting the left foot is defined as follows:

$$\begin{cases} \min(x) = -0.3 \text{ m} \\ \max(x) = +0.3 \text{ m} \\ \min(y) = 0 \\ \max(y) = +0.3 \text{ m} \\ \min(z) = z_{\min} \text{ (minimum value in the } z \text{ direction)} \\ \max(z) = z_{\min} + 0.075 \text{ stature} \end{cases}$$

To delimit the hands, the tips of the middle fingers of both hands are first identified. These features correspond to extremities in the Y direction as shown in Fig. 4. For example, the box corresponding to the right hand is located using the tip of the middle finger (midd_r) as follows:

$$\begin{cases} \min(x) = \text{midd}_r(x) - 0.1 \\ \max(x) = \text{midd}_r(x) + 0.1 \\ \min(y) = \text{midd}_r(y) \\ \max(y) = \text{midd}_r(y) + 0.15 \\ \min(z) = \text{midd}_r(z) \\ \max(z) = \text{midd}_r(z) + 0.2 \end{cases}$$

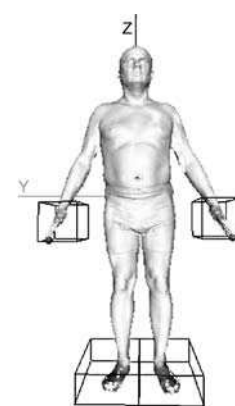


Fig. 4. Segmentation of the feet and hands

The head is approximately identified by points having a Z-coordinate exceeding a threshold that we set to 85% of the stature.

4.4 Filling holes on horizontal slices

4.4.1 Converting a polygonal surface to horizontal slices and identifying hole boundaries on each slice

The human models are sliced by intersecting horizontal planes with the edges of the surface triangles. Points of intersection that belong to the same triangle are then connected with a line segment. We identify hole boundaries as points that are connected to at most one other point. In order to fill the holes in the model, we propose to connect these points so that each slice is converted to a set of closed curves.

4.4.2 Connecting the hole boundaries

Let \mathcal{P}_k be the set of points corresponding to the hole boundaries in the slice k . The main issue in generating closed curves in each slice is to find the optimal way of connecting the boundary points. To solve this problem we use two criteria. The first one tends to connect points that are close to each other. The second criteria aims to preserve the curvature of the measured data by prioritizing the connection of points that have similar orientation of the normal to the surface. This criterion minimizes the possibility of bridging body parts beyond branching points. The two criteria are expressed in the form of a cost function C_k that has to be minimized in order to find the optimal way of connecting the hole boundaries.

We formulate the cost function differently depending on whether the slice belongs to the feet, the head or the rest of the body.

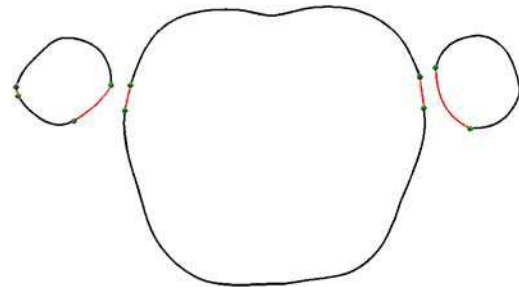


Fig. 5. Hole-filling of a slice. Black curves correspond to original data and red curves correspond to estimated data

The cost of connecting points that belong to the feet or the head is given by:

$$C_k = \sum_{i,j \in \mathcal{P}_k} \{\|p_i - p_j\| + (1 - \cos(\mathbf{n}_i, \mathbf{n}_j))\}. \quad (1)$$

Where p_i and \mathbf{n}_i represent the position of the point i and its corresponding normal to the surface, respectively.

The cost of connecting points from the rest of the body is given by:

$$C_k = \sum_{i,j \in \mathcal{P}_k} \{\|p_i - p_j\| * (1 - \cos(\mathbf{n}_i, \mathbf{n}_j))\}. \quad (2)$$

The second function attributes more importance to the similarity between the orientations of the normal to the surface. In fact, the cost of connecting two points that have the same normal orientation is zero regardless of how distant they are. This function avoids creating bridges between body parts beyond the branching points.

In order to identify the optimal way of connecting the boundary points, we evaluate the cost of all the connections that satisfy the following conditions:

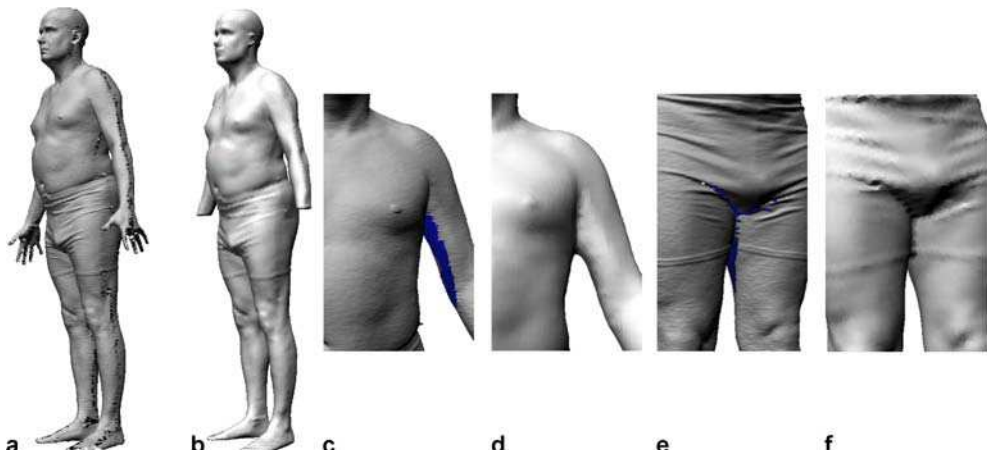


Fig. 6a-f. Repairing of a CAESAR human model. **a, c, and e** Original model, **b, d, and f** repaired model

- The distance between two connected points does not exceed a maximum distance.
- A connection between two points is invalid if it intersects with another segment from the slice.
- All the points should be connected.

After determining the optimal connections, simply connecting the hole boundaries with line segments does not provide an adequate approximation of the missing body parts, especially if the connected points are far apart from each other. For this reason we propose to connect the hole boundaries with second-order Bezier curves. These curves have the advantage of preserving the curvature of the measured data.

4.5 Voxelization

Voxelization based on a signed distance map consists of two steps. The first step classifies each voxel as lying in the interior or the exterior of the body. The second step computes the distance from each voxel to its nearest surface point.

4.5.1 Voxel classification

For manifold polygonal models that are watertight, a voxel can be classified by counting the number of times that a ray with its origin at the centre of the voxel intersects polygons of the model (parity count). An odd number of intersections corresponds to an interior voxel and an even number corresponds to an exterior voxel. In our implementation, voxelization is performed after slicing the surface. Therefore, rays are intersected with slices rather than with the model surface.

For some slices where the data is extremely noisy, the criteria used in our hole-filling algorithm are not sufficient to connect the boundary points appropriately. Thus, voxels can be misclassified. To overcome this limitation, we use different directions for scan-converting models as proposed in [16]. Each direction votes on the classification of a voxel and the majority vote is the voxel's final classification.

4.5.2 Computing distances of voxels to the surface

Accurately computing the distance from the centre of each voxel to its nearest surface point is time-consuming. So far, polygonal models are converted to slices. Each slice is a set of connected segments. This fact is useful, since computing the distance to a segment is faster than computing the distance to a triangle. Moreover, we adopt the following measures to reduce the computation time:

- Approximation of the distance: A fast approximation of the distance field \tilde{dist} is first determined using the Danielson algorithm [5]. The accurate distance is then computed only for voxels that are within a certain distance from the body surface. The Danielson algorithm

starts from a binary volumetric representation where voxels are classified either as feature or non-feature voxels. The algorithm computes the distance of each non-feature voxel to the nearest feature voxel by propagating the distances in a small neighbourhood. In order to compute distances of both interior and exterior voxels, the Danielson algorithm is applied twice to generate an estimated distance for each voxel. In the first pass, feature voxels correspond to the interior and the surface voxels, while in the second pass, feature voxels correspond to exterior and surface voxels.

- Reducing the number of segments with which the distance has to be computed: For each voxel V we start with identifying the distance ds to the closest segments from the same slice. Only segments that are inside a square around V and having a diagonal equal to $2dist$ are considered. After identifying ds , segments from other slices that are inside a cube around V and having a diagonal equal to $2ds$ are considered. Positive distances are assigned to interior voxels and negative distances are assigned to exterior voxels. A complete surface model is then extracted from the volumetric description using the marching cubes algorithm [14].

Figure 6 illustrates a human model after hole-filling. The surface is extracted from a volumetric representation with a sampling rate of 8 mm. The result shows that most of the holes in the original models are properly filled, except for areas such as the ears where most of the information is missing.

5 Principal components analysis

To apply PCA to the volumetric models, we form a vector, Ψ , for each model, where each element of the vector is the signed distance from a voxel to the surface of the model. The average over N models is given by $\bar{\Psi} = (1/N) \sum_{i=1}^N \Psi_i$. The deviation vectors $\Phi_i = \Psi_i - \bar{\Psi}$ are arranged in a matrix $\mathbf{A} = [\Phi_1 \Phi_2 \cdots \Phi_N]$. The PCA of the matrix \mathbf{A} generates a set of non-correlated eigenvectors \mathbf{u}_i and their corresponding variances λ_i . The eigenvectors are sorted according to the decreasing order of their variances. Each vector Φ_i can be approximated as

$$\hat{\Phi}_i \approx \sum_{j=1}^M c_{ij} \mathbf{u}_j, \quad (3)$$

where $0 \leq M \leq N$ and $c_{ij} = \Phi_i \cdot \mathbf{u}_j$. In other words, every model can be reconstructed by the linear combination of a subset of the eigenvectors. The quality of the reconstruction can be evaluated by the fraction $\sum_{i=1}^M \lambda_i / \sum_{i=1}^N \lambda_i$, representing the percentage of the variance spanned by the eigenvectors chosen for the reconstruction.

6 Reconstruction

PCA is applied to 300 male subjects from the CAESAR database. Only the standing posture is considered in our experiments. The models are first converted to a volumetric representation. PCA extracts a set of eigenvectors that represent an orthogonal basis of the human shape space inside the studied models. The eigenvectors are arranged according to the decreasing order of the percentage of the shape variability that they induce. Experimental results show that the first 64 eigenvectors represent 95% of

the total variance. Figure 7 illustrates three examples of the reconstructed models using Eq. 3. For visualization purposes, we convert the volumetric models back to the surface meshes using the marching cubes algorithm [14]. As we can see, even with a reduced number of coefficients, the global geometry of the reconstructed body shapes are fairly close to the original scans.

7 Interpretation of main modes of variation

The first few eigenvectors extracted by applying PCA to a set of human models represent the main modes of shape variation within the studied population. In this section, we visualize the first five modes of variation and give interpretations of these modes, linking them to some intuitive body shape variations. This information is important for many applications, for example, the design of products that interact with humans.

To visualize the main modes of the shape variation, we start with projecting a real model onto the basis of main components. For each mode of variation, we generate a sequence of virtual models by changing the coefficient of correlation with the corresponding eigenvector, while keeping the rest of the coefficients constant. The sequence of virtual models show only the shape variation that is induced by the corresponding mode of variation. The interpretations of these modes are made obvious by animating the virtual models. Representative virtual models are presented and compared with the real models with the same range of coefficients.

We conducted three groups of experiments. In the first group, we apply PCA to the original models. In the second group, we normalize models to the same height before applying PCA. There are two reasons for the normalization. One is that it isolates the shape variation from the height variation. Another is that it improves the correspondences between the models, because if the models are at the same height, their anatomical components tend to align better with each other. After normalizing the height, the arms represent the body segments where the misalignment is the most severe and in some extreme examples a model's arm can correspond to part of another model's torso. These misalignments introduce artificial variability that does not reflect the changes of the body shape. Therefore, in the third group of experiments we eliminate the arms.

In the following interpretations we concentrate on the overall body shape variation and ignore the details on the heads. Our method can be applied to the heads separately. Tables 1 and 2 summarize the interpretations of the first five modes under non-normalized and normalized conditions, respectively.

In 1940, Sheldon et al. [21] proposed three components for characterizing the human body: endomorphy (soft and roundness), mesomorphy (hardness and muscu-

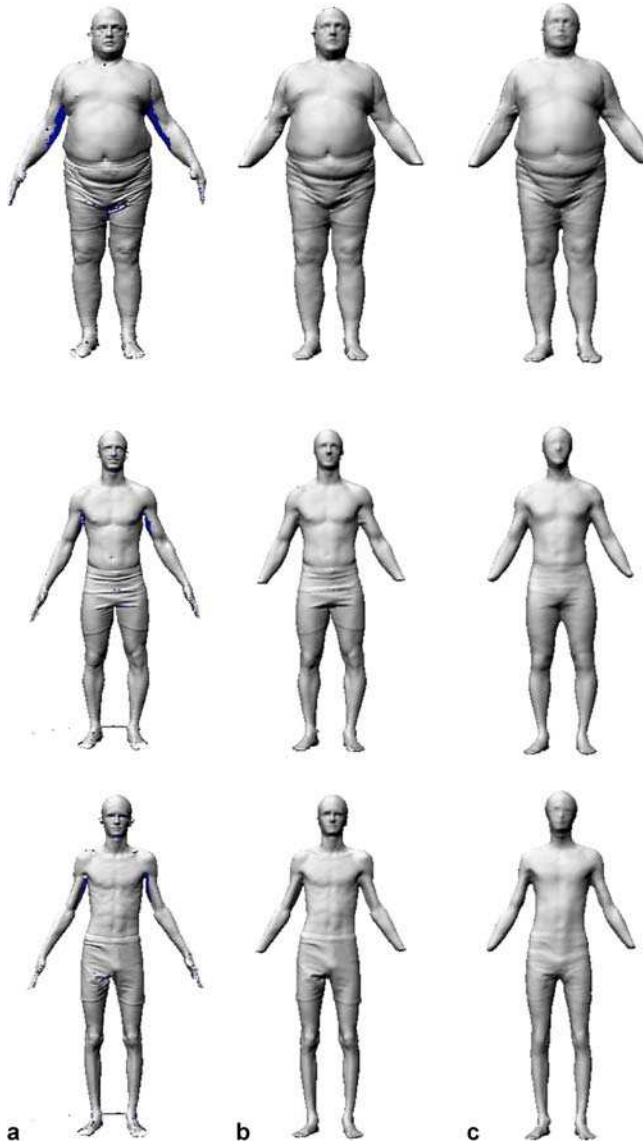


Fig. 7a–c. Reconstruction of human models using the first 64 eigenvectors extracted from the volumetric representation of 300 male subjects. **a** Original models; **b** repaired models; **c** reconstructed models

Table 1. Non-normalized

| Mode | Interp. | Variability |
|------|---------------------|-------------|
| 1st | weight & height | 35.0% |
| 2nd | $weight/(height)^3$ | 15.0% |
| 3rd | alignment artifact | 9.53% |
| 4th | leaning posture | 4.02% |
| 5th | muscularity | 3.17% |

Table 2. Normalized

| Mode | Interp. | Variability |
|------|-------------------|-------------|
| 1st | weight | 33.86% |
| 2nd | leaning posture | 15.11% |
| 3rd | muscularity | 8.93% |
| 4th | arm-torso spacing | 4.0% |
| 5th | head position | 3.64% |

larity) and ectomorphy (linearity and skinniness). Our interpretations can be considered as a generalization of these components. While Sheldon et al.'s observations are qualitative, we provide quantitative measurements.

7.1 Non-normalized models

The modes of variation are presented in decreasing order of the percentage of the variability they induce.

7.1.1 First mode

The first mode of variation, representing 35% of the total shape variability within the studied set of models, reflects a combination of height and weight (but is dominated by height). In Fig. 8, we arrange models in increasing order of their projection on the first main component. One side

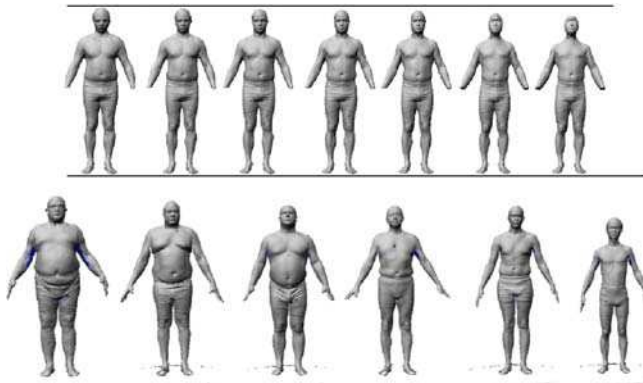


Fig. 8. First mode of variation without height normalization (35.01% of the total shape variability). This mode represents a combination of height and weight variation. First row: virtual models; second row: original models

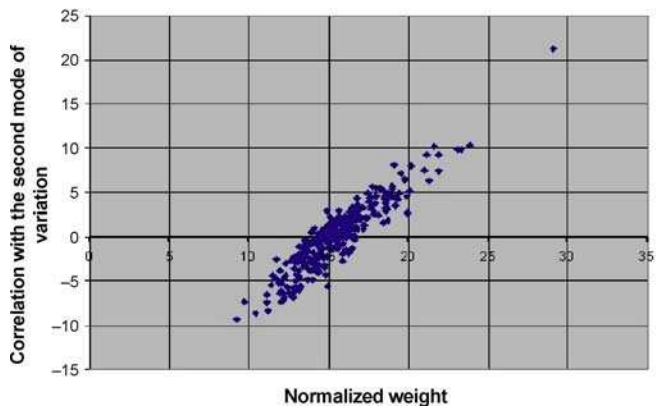


Fig. 9. Correlation between the second mode of variation and the normalized weight

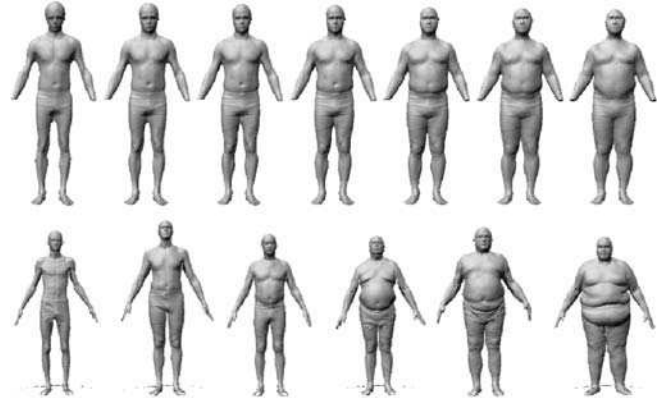


Fig. 10. Second mode of variation without height normalization. This mode is correlated to the normalized weight ($weight/(height)^3$)

of the mode represents tall and wide persons and the other side represents short and thin ones.

7.1.2 Second mode

The second mode of variation is highly correlated to the normalized weight, which we define as the ratio of the weight and the cube of the height. In Fig. 9, each dot represents a model with the horizontal axis as the normalized weight and the vertical axis as the correlation with the second mode of variation. This mode of variation represents 15% of the global variance. Figure 10 shows that the model changes from thin on the left to wide on the right.

7.1.3 Third mode

The third mode of variation does not seem to correspond to any anatomical variation. It is rather an artifact that is due to the misalignment in the upper body (Fig. 11).

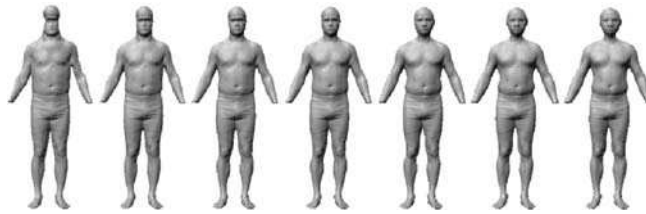


Fig. 11. Third mode of variation without height normalization. This mode of variation corresponds to artifacts due to the misalignment

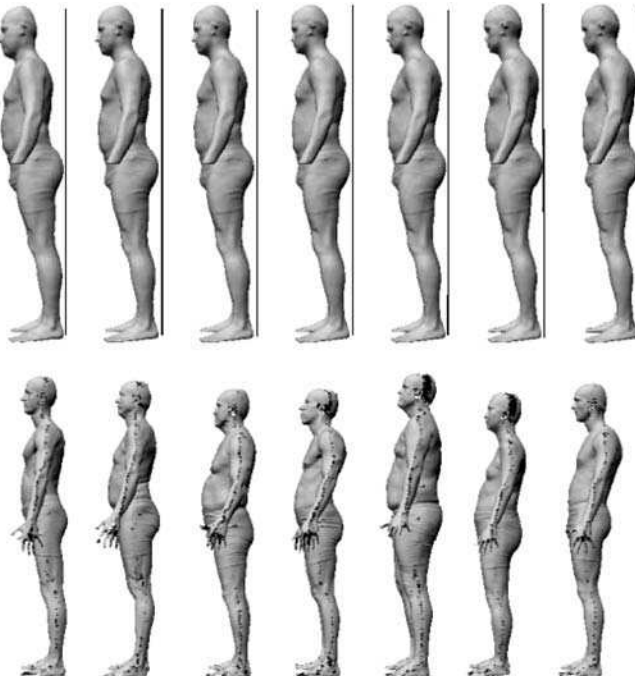


Fig. 12. The fourth mode of variation without height normalization. This mode reflects a posture variation. The posture varies from bending forward to leaning backward

7.1.4 Fourth mode

The fourth mode of variation corresponds to a posture variation (Fig. 12). The models vary from a posture of bending forward to a posture of leaning slightly backward.

7.1.5 Fifth mode

The fifth mode of variation represents a difference of muscularity and distribution of mass between the torso and the legs (Fig. 13). From one side of the component, models have a large abdomen, narrow hips, and close thighs. When the correlation to the fifth mode increases, the models tend to become more muscular with larger hips and thighs that are farther apart. This mode of variation is comparable to the ectomorph component of the Sheldon representation [21].

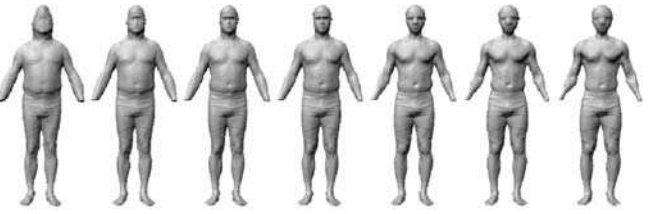


Fig. 13. Fifth mode of variation without height normalization. This mode reflects a variation of muscularity and a distribution of mass between the torso and the legs

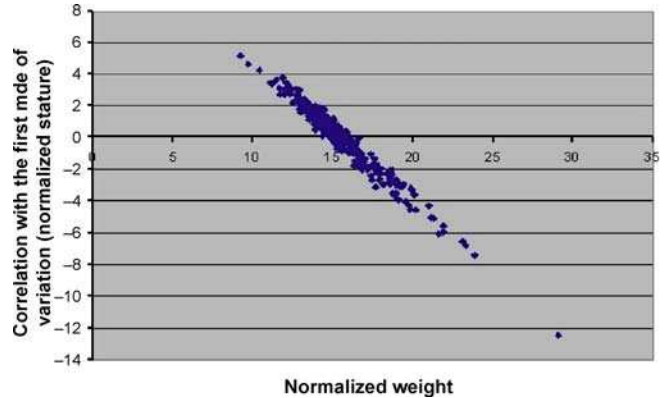


Fig. 14. Correlation between the first mode of variation and the normalized weight

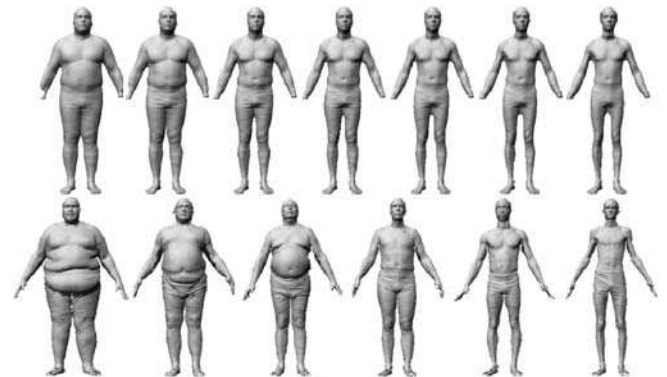


Fig. 15. First mode of variation for normalized models. This mode reflects the weight variation representing 34% of the global variability

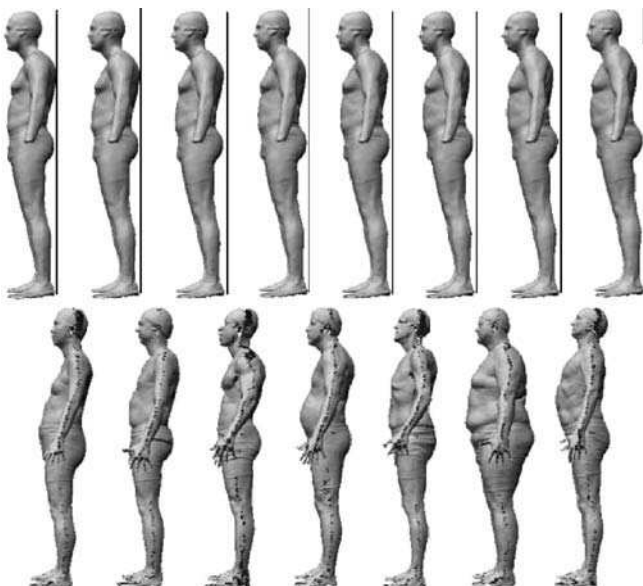


Fig. 16. Second mode of variation with height normalization

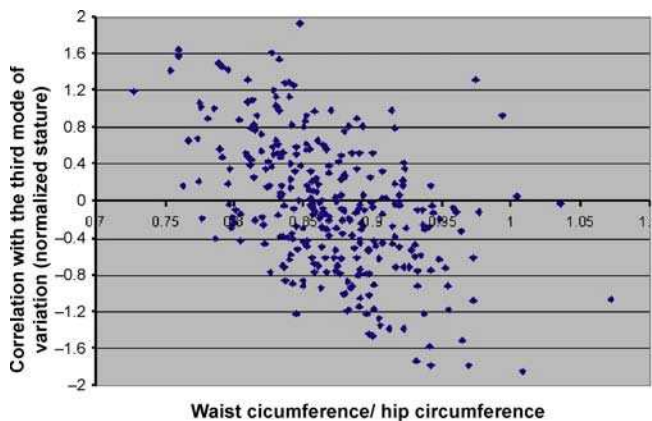


Fig. 17. Correlation between the third mode of variation and the waist/hip circumference ratio

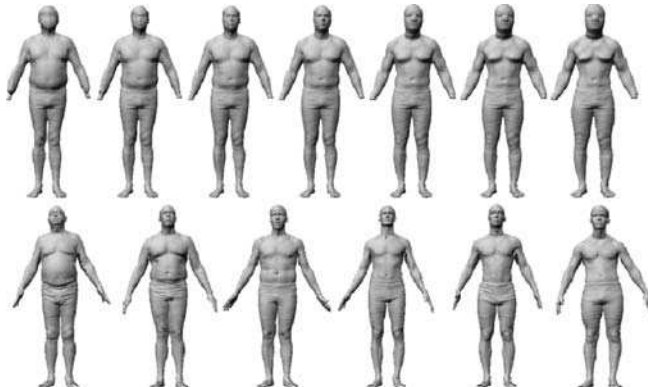


Fig. 18. Third mode of variation (normalized)

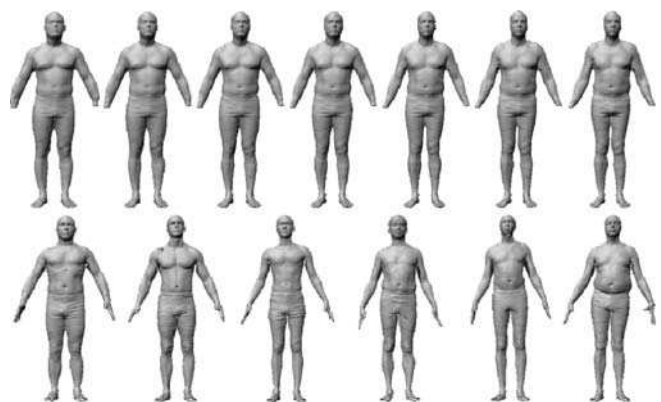


Fig. 19. Fourth mode of variation (normalized)

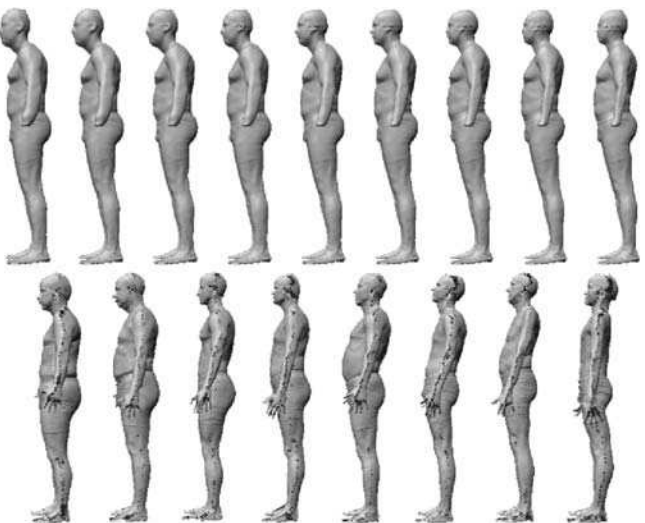


Fig. 20. Fifth mode of variation (normalized)

7.2 Normalized models

The application of PCA to the volumetric representation of non-normalized models extracts modes such as the variation of height, weight, posture, and muscularity. However the misalignment between the models generates such artifacts as we have seen in the third component. Normalizing the height of the models to the same value reduces the misalignment in the upper body and thus improves the correspondence provided by the volumetric representation.

7.2.1 First mode

Not surprisingly, after normalizing the height, the first mode of variation is weight. As shown in Fig. 15, this mode of variation, representing 33.86% of the global variability, is equivalent to the second component for the non-

normalized models. Notice that the models change from wide to thin as we increase the coefficients, whereas in the non-normalized situation (Fig. 10), the direction of change is from thin to wide. This is because the direction of the eigenvectors can be both ways.

The correlation of this mode with the normalized weight is illustrated in Fig. 14.

7.2.2 Second mode

The second mode of variation is equivalent to the fourth mode of variation in the non-normalized models. It reflects a posture variation where the models are bending forward on the one side and leaning backward on the other (Fig. 16). This mode of variation represents 15.11% of the global variability.

7.2.3 Third mode

The third mode of variation represents 8.93% of the global variability. This component corresponds to a variation of mass distribution and muscularity (Fig. 18). It is equivalent to the fifth mode in the non-normalized models. Figure 17 illustrates a correlation between this mode and the waist/hip circumference ratio. We notice that for low correlation coefficients, the waist circumference is larger than the hip circumference, whereas for high coefficients the hips are larger.

7.2.4 Fourth mode

The fourth mode of variation represents 4% of the global variability. It reflects a variation of the spacing between the arms and the torso. In addition, this mode also corresponds to the proportional lengths between the upper and lower body. From Fig. 19, we observe that the legs of the models become longer as we increase the correlation coefficient.

7.2.5 Fifth mode

The fifth mode represents 3.64% of the global variation. It corresponds to a variation of the head position relative to the rest of the body. When the head is leaning backward, the back of model tends to have an arch (Fig. 20).

7.3 Models with segmented arms

The first five modes extracted from the models with segmented arms are similar to the ones extracted in the previous experiment, except for the variation corresponding to the arms (Fig. 21). However, the percentages of variability associated to these modes are slightly different from the previous ones. The first five modes of variation represent 36.15%, 9.5%, 6.29%, 5.26%, and 4.61% of the total variability.

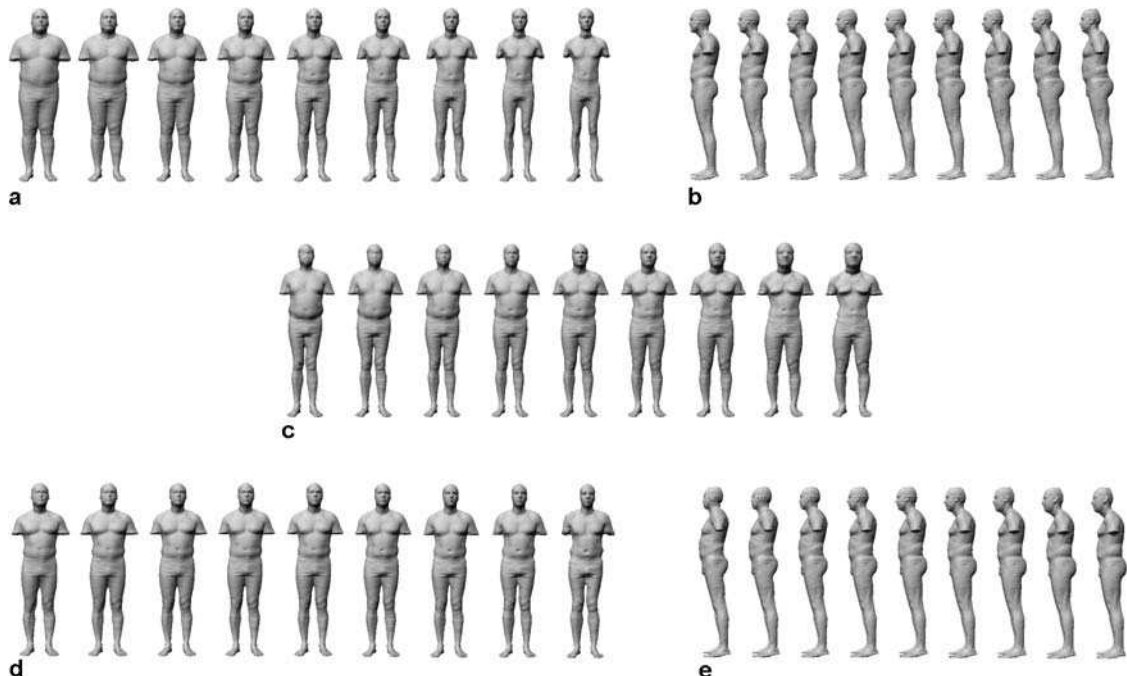


Fig. 21. The first five modes of variation after eliminating the arms

8 Conclusions

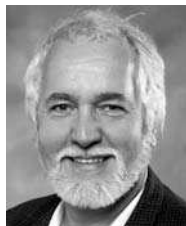
This paper introduces a new approach to anthropometric measurement based on 3D scanning technology. Using the distance functions computed on the volumetric representation of 3D models, we have shown that an extensive human body shape analysis can be performed by principal components analysis without knowledge of the anatomical landmarks. We applied PCA to 300 male subjects from the CAESAR database to extract the main modes of variation of the human body shape. In particular, we have shown that the human body shape can be globally

represented with a small number of principal components. Furthermore, we have found that the first few components represent meaningful intuitive body variations. We have given interpretations to the first five components—some of them provide quantitative evidence to the empirical anthropometric observations [21].

Our interpretations have not been validated by the experts in the fields of anthropometry, anatomy, and anthropology. Nevertheless, this new approach provides powerful tools for these fields and our study is only the first step toward a fast and more reliable characterization of the whole human body.

References

1. Allen, B., Curless, B., Popović, Z.: The space of human body shapes: reconstruction and parametrisation from range scans. *ACM Trans. on Graph. (ACM SIGGRAPH'2003)* **22**(3), 587–594 (2003)
2. Azouz, Z.B., Rioux, M., Lepage, R., Shu, C.: Compact description of human body shape using extended hyperquadrics. *Proceedings of the 15th Triennial Congress of the International Ergonomics Association*, Seoul, Korea (2003)
3. Burnsides, D., BoehmerK, M., Robinette, K.: 3-D landmark detection and identification in the caesar project. In: *Proceedings of the Third International Conference on 3D Digital Imaging and Modeling (3DIM'2001)*, pp. 393–398. Quebec City, Canada (2001)
4. Carr, J., Beatson, R., Cherrie, J., Mitchell, T., Fright, W., McCallum, B., Evans, T.: Reconstruction and representation of 3d objects with radial basis functions. In: *Proceedings of ACM SIGGRAPH 2001*, pp. 67–76 (2001)
5. Danielsson, P.E.: Euclidean distance mapping. *Computer Graphics and Image Processing* **14**(3), 227–248 (1980)
6. Davis, J., Marschner, S., Garr, M., Levoy, M.: Filling holes in complex surfaces using volumetric diffusion. In: *Proceedings of the First International Symposium on 3D Data Processing, Visualization and Transmission*. Padua, Italy (2002)
7. Inc., C.: <http://www.cyberware.com>
8. Inc., I.: <http://www.innovmetric.com>
9. Inc., V.: <http://www.vitronic.com>
10. Jones, M.: The production of volume data from triangular meshes using voxelization. *Comput. Graph. Forum* **15**(5), 311–318 (1996)
11. Kaufman, A.: An algorithm for 3d scan conversion of polygons. In: *Proceedings of EUROGRAPHICS'87*, pp. 197–208. North Holland, Amsterdam (1987)
12. Kaufman, A.: Volume visualization (tutorial). *IEEE Computer Society Press*, Washington DC (1991)
13. Kirby, M., Sirovich, L.: Application of the Karhunen-Loeve procedure for the characterisation of human faces. *IEEE Trans. Patt. Anal. Mach. Intell.* **12**(1), 103–108 (1990)
14. Lorensen, W., Cline, H.: Marching cubes: a high resolution 3-D surface construction algorithm. *Proc. SIGGRAPH 1987* **21**(3), 163–169 (1987)
15. Magnenat-Thalmann, N., Seo, H.: Automatic modeling of animatable virtual humans- a survey. *Fourth International Conference on 3D Digital Imaging and Modeling*, IEEE Computer Society, pp. 2–10 (2003)
16. Nooruddin, F., Turk, G.: The production of volume data from triangular meshes using voxelization. *IEEE Trans. Visual. Comput. Graph.* **9**(2), 191–205 (2003)
17. Paquet, E., Robinette, K., Rioux, M.: Management of three-dimensional and anthropometric databases: Alexandria and Cleopatra. *J. Electron. Imaging* **9**(4) (2000)
18. Robinette, K., Daanen, H., paquet, E.: The CAESAR project: A 3-D surface anthropometry survey. In: *Second International Conference on 3D Digital Imaging and Modeling (3DIM'99)*, pp. 380–386. Ottawa, Canada (1999)
19. Robinette, K., Vannier, M., Rioux, M., Jones, P.: 3-D surface anthropometry: review of technologies = L'anthropométrie de surface en trois dimensions: examen des technologies. In: Neuilly-sur-Seine: North Atlantic Treaty Organization Advisory Group for Aerospace Research & Development, Aerospace Medical Panel (1997)
20. Seo, H., Magnenat-Thalmann, N.: An automatic modeling of human bodies from sizing parameters. *SIGGRAPH Symposium on Interactive 3D Graphics*, pp. 19–26 (2003)
21. Sheldon, W., Stevens, S., Tucker, W.: The varieties of human physique. Harper and Brothers Publishers, New York (1940)
22. Stralen, M., Daanen, H., Tangelder, J.: A tool box to identify holes in 3d human body scans. In: *Proceedings of the 15th Triennial Congress of the International Ergonomics Association (IEA 2003)*. Seoul, Korea (2003)
23. Taubin, G.: Geometric signal processing on polygonal meshes. *EUROGRAPHICS'2000* (2000)
24. Wang, S., Kaufman, A.: Volume sampled voxelization of geometric primitives. *Proceedings of the 4th Conference on Visualization'93*, San Jose, California, pp. 78–84 (1993)



ZOUHOUR BEN AZOUZ received her PhD from the Department of Automated Production, École de Technologie Supérieure de Montréal in 2005. She received her Master's degree in automation and computer-integrated manufacturing in 1997 from Institut National Polytechnique de Grenoble (INPG) and a degree in electrical engineering in 1996 from Ecole Nationale d'ingénieurs de Tunis. She is currently research associate at the National Research Council of Canada. Her research has mostly been in human shape modeling.

MARC RIOUX is a principal research officer of the Institute for Information Technology at the National Research Council Canada. His present interests are in the development of three-dimensional digitizing, modeling and display for machine vision, optical dimensional inspection and visual communication in the Visual Information Technology Group. He received his bachelor's degree in engineering physics in 1971

and a master's degree in physics in 1976, both from Laval University. He worked five years on CO₂ laser development and applications and two years in infrared holography and joined the National Research Council in 1978 to work on 3D digitizing.

CHANG SHU received a PhD in computer science from Queen Mary College, University of London, UK, in 1992, and a BSc from Harbin Institute of Technology, China, in 1985. He is currently a senior research scientist at the Institute for Information Technology, National Research Council of Canada. He is also an adjunct research professor at the School of Computer Science, Carleton University, Ottawa, Canada. From 1992 to 1996, he was a research associate in the Department of Mechanical and Aerospace Engineering at the Carleton University. His research has mostly been in developing geometric methods for solving problems in computer vision, computer graphics, robotics, and scientific

computing. His current research interests include surface reconstruction, human shape modeling, and augmented reality. He is a member of the IEEE.

RICHARD LEPAGE received the degree in electrical engineering in 1974, the M.S. degree in signal processing in 1982, and the Ph.D. degree in applications of artificial neural networks to computer vision, in 1994, all from Laval University, Quebec, P.Q., Canada. He is currently a professor in the Department of Automated Production, École de Technologie Supérieure, Université du Québec, Montréal, P.Q. From 1976 to 1989, he was with the Defense Research Center, Montréal, Canada. His research interests include neural networks, computer vision, 3D vision, automated inspection systems, and quality insurance in agro foods with the aid of artificial intelligence.